Saudi Pharmaceutical Journal 27 (2019) 1025–1035

Contents lists available at ScienceDirect

Saudi Pharmaceutical Journal

journal homepage: www.sciencedirect.com

Biocompatibility and paclitaxel/cisplatin dual-loading of nanotubes prepared from poly(ethylene glycol)-polylactide-poly(ethylene glycol) triblock copolymers for combination cancer therapy

Xin Shen [a,b], Yuandou Wang [b], Laishun Xi [c], Feng Su [c,*], Suming Li [d,*]

[a] Cancer Institute, The Affiliated Hospital of Qingdao University, Qingdao 266061, China
[b] Institute of High Performance Polymers, Qingdao University of Science and Technology, Qingdao 266042, China
[c] State Key Laboratory Base of Eco-chemical Engineering, College of Chemical Engineering, Qingdao University of Science and Technology, Qingdao 266042, China
[d] Institut Européen des Membranes, UMR CNRS 5635, Universitéde Montpellier, 34095 Montpellier, France

ARTICLE INFO

Article history:
Received 3 May 2019
Accepted 30 August 2019
Available online 30 August 2019

Keywords:
Nanotubes
Block copolymer
Combination cancer therapy
Biocompatibility
Drug delivery

ABSTRACT

Nanotubes were prepared by self-assembly of the copolymer using co-solvent evaporation method. The biocompatibility of the nanotubes was assessed in comparison with spherical micelles and filomicelles prepared from poly(ethylene glycol)-poly(L-lactide-co-glycolide) (PEG-PLGA) and poly(ethylene glycol)-poly(L-lactide) (PEG-PLA), respectively. Several aspects of biocompatibility of the aggregates were considered, including agar diffusion and MTT assay, release of cytokines, hemolysis, protein adsorption, dynamic clotting *in vitro*, and Zebrafish embryonic compatibility *in vivo*. The nanotubes present good cell compatibility and blood compatibility *in vitro*, and almost no toxicity towards Zebrafish embryos development *in vivo*. Furthermore, dual-loading of hydrophilic cisplatin and hydrophobic paclitaxel was achieved in the nanotubes with high loading content and loading efficiency. The release of both drugs was slower from dual-loaded nanotubes than from single-loaded ones, but the total amount of released drugs in higher for dual-loaded nanotubes than from single-loaded ones. Cellular uptake and inhibition tests showed that the nanotubes were successfully taken up by tumor cells and effectively inhibited cell growth. It is thus concluded that PEG-PLA-PEG nanotubes with outstanding biocompatibility could be promising for co-delivery of hydrophilic and hydrophobic agents in combination cancer therapy.

1. Introduction

Biodegradable polymers, and in particular polylactide (PLA) and poly(lacitde-co-glycolide) (PLGA) have been widely studied in the past decades for biomedical applications such as drug delivery systems (DDS), surgical sutures, internal fixation devices, and tissue engineering scaffolds due to their excellent biocompatibility and degradability (Li et al., 2016a,b). A number of PLA- or PLGA-based medical devices and DDS have been approved for clinical uses by the FDA (Zhang et al., 2013). Meanwhile, poly(ethylene glycol) (PEG) is commonly used in various forms of DDS because of its excellent physicochemical and biological properties such as water solubility, low-toxicity and anti-protein adsorption or cell adhesion to minimize the activation of immune systems and thereby increase circulation time of DDS in the bloodstream. It has been proved that due to the enhanced permeability and retention (EPR) effect, long-circulating vectors preferentially accumulate in solid tumors (Xiong et al., 2016a,b).

Amphiphilic copolymers comprising hydrophilic block like PEG and degradable hydrophobic polyester block like PLA have been largely investigated as potential drug vector (Tyler et al., 2016). They can self-assemble in aqueous environment to yield aggregates having a variety of structures such as spherical micelles, polymersomes, filomicelles and nanotubes (Wauters et al., 2018; Jelonek et al., 2015). Artificial hollow aggregates, and especially nanotubes have recently attracted much interest as novel drug carrier (Harada and Discher, 2011). In fact, nanotubes can achieve long circulation time similar to filomicelles (Loverde et al., 2011). They also exhibit higher drug encapsulation ability in comparison with spherical micelles because the core volume is larger. Moreover,

* Corresponding authors.
E-mail addresses: sufeng@qust.edu.cn (F. Su), suming.li@umontpellier.fr (S. Li).
Peer review under responsibility of King Saud University.

Production and hosting by Elsevier

https://doi.org/10.1016/j.jsps.2019.08.005
1319-0164/

nanotubes are able to encapsulate both hydrophobic and hydrophilic drugs because of the co-existence of internal hydrophilic region and intermediate hydrophobic region within the architecture. In fact, DDS loaded with two or more drugs could present a synergistic therapeutic effect in treating cancers. Ahmed et al. reported on PEG-PLA polymersomes for the co-delivery of paclitaxel (PTX) and doxorubicin (DOX) (Ahmed et al., 2006). The cell death induced by polymersomes in tumors was twice higher than free drugs and showed a similar increase in maximum tolerable dose and drug accumulation within the tumor. PEG-PLGA copolymer nanoparticles were loaded with PTX and cisplatin (CDDP), and enhanced anti-tumor effect was observed (Wu et al., 2014). PEG-polypeptide nanoparticles loaded with DOX and PTX were also used to evaluate the synergistic antitumor efficacy *in vitro* and *in vivo* (Lv et al., 2014).

Biocompatibility is of major importance for applications of biomaterials in medical and pharmaceutical fields. In the case of DDS, it refers to their ability to perform designed functions in drug therapy without causing undesired reactions (Williams, 2008). Recently, the biocompatibility of PEG-PLA filomicelles and PEG-PLGA spherical micelles in solution was reported (Liu et al., 2018a,b; Shen et al., 2017). In fact, the architecture of self-assembled aggregates of amphiphilic copolymers mainly depends on the hydrophilic/hydrophobic ratio, the chain structure (AB, ABA or BAB-type) and structural regularity of the hydrophobic block. Various architectures such as spherical micelles, rod-like micelles, filomicelles, polymersomes and nanotubes are obtained from PEG-PLA, PEG-PLGA and PEG-PLA-PEG copolymers (Liu et al., 2018a,b; Shen et al., 2017; Wu et al., 2013). In particular, asymmetric PEG-PLA-PEG copolymers are susceptible to self-assemble to yield polymersomes or nanotubes (Wu et al., 2013).

In this work, nanotubes were prepared by self-assembly of an asymmetric PEG-PLA-PEG copolymer. The biocompatibility of nanotubes was assessed in comparison with spherical micelles and filomicelles obtained from PEG-PLGA and PEG-PLA copolymers, respectively. Various aspects of cell and blood compatibility *in vitro* and Zebrafish embryonic compatibility *in vivo* were considered. Single and dual-loaded drug release, cellular uptake and inhibition of nanotubes were studied to assess the potential of nanotubes as drug carrier in combination cancer therapy

2. Materials and methods

2.1. Materials

Poly(ethylene glycol) methyl ether (mPEG), *L*-lactide, glycolide, thiazolyl blue tetrazolium bromide (MTT), phorbol-12-myristate-13-acetate (PMA) were obtained from Sigma-Aldrich. Dulbecco's Modified Eagle Medium (DMEM), RPMI Medium 1640, Fetal Bovine Serum (FBS) were purchased from Gibco. Other organic solvents were of analytic level from Sinopharm Chemical Reagent Co. (SCRC). PEG-PLA-PEG (Wu et al., 2013), PEG-PLA (Shen et al., 2017), PEG-PLGA (Liu et al., 2018a,b) were synthesized as previously described.

2.2. Preparation and characterization of aggregates

Aggregates of copolymers were obtained by using co-solvent evaporation method (Jelonek et al., 2016). 5 mg copolymer was dissolved in 100 μL chloroform. Then 5 mL distilled water was introduced. The solution was mixed by vigorous stirring for 3 h, followed by gentle stirring overnight for evaporation of solvent.

The morphology of aggregates was visualized through transmission electron microscopy (TEM) on JEOL JEM-2100. The size and distribution of spherical micelles were determined by using dynamic light scattering (DLS) performed on Malvern Zetasizer Nano ZS90.

2.3. Cytocompatibility evaluation

2.3.1. Agar diffusion assay

Agar diffusion was carried out to determine the cell toxicity as recommended by ISO 10993-5. L-929 mouse fibroblasts were cultured in plastic Petri dishes (90 mm). The medium was removed and replaced by 1.5% nutrient agar after 24 h. Neutral red solution at a concentration of 0.1 mg/mL in phosphate buffered saline (PBS) was prepared to stain living cells. Aggregate solutions at 1 mg/mL was dropped to a 5 mm diameter filter paper and placed on the petri dish for 24 h to measure the degree of shrinkage and decolorization, using the medium as negative control and phenol solution at 6.4% as positive control.

2.3.2. MTT assay

The MTT test has been developed as a screening method for cytotoxicity assessment of biomaterials *in vitro*. Aggregate solution at concentrations of 0.05, 0.1, 0.2, 0.5 and 1.0 mg/mL with medium containing 10% calf serum were exposed to L-929 and human umbilical vein endothelial cells (HUVEC), respectively. After predetermined time intervals, 20 μL MTT at 5 mg/mL was introduced for 6 h incubation. Then the medium was removed, and 150 μL dimethyl sulfoxide (DMSO) was added. After 10 min shaking, the optical density (OD) was determined using microplate reader at 570 nm (Elx800; BioTek, USA). 100 μL solution of phenol in water was used as positive control, and 100 μL fresh medium as negative control. The relative activity of cells was calculated using the following formula:

$$\text{Relative activity}(\%) = (\text{OD}_{\text{test sample}}/\text{OD}_{\text{negative control}}) \times 100 \quad (1)$$

2.3.3. Inflammatory cytokine release analysis

Human monocytic leukemia cell line THP-1 monocytes were induced to macrophages by culture with PMA at 100 ng/mL for 48 h. 100 μL aggregate solution at 1 mg/mL was exposed to macrophages for 24 h, using a mixture of RPMI 1640 and phenol in water as positive control, and a mixture of RPMI 1640 and physiological saline as negative control. The release profiles of cytokines, including tumor necrosis factor (TNF-α), interleukin (IL-1β) and transforming growth factor (TGF-β1) were determined using ELISA kits.

2.4. Hemocompatibility assessment

2.4.1. Hemolysis test

10 mL aggregate solution at 1 mg/mL was introduced to a silanized beaker, and preheated at 37 °C for 30 min. Then 0.2 mL diluted rabbit acid-citrate-dextrose (ACD) blood was introduced and incubated for 60 min. Physiological saline was used as negative control, and distilled water as positive control (Gao et al., 2010). The solution was centrifuged and the supernatant was collected to determine the OD value at 540 nm. Hemolytic ratio (HR) of aggregate solutions was calculated using the following formula:

$$\text{HR}(\%) = \left[(\text{OD}_{\text{test}} - \text{OD}_{\text{negative}})/(\text{OD}_{\text{positive}} - \text{OD}_{\text{negative}})\right] \times 100 \quad (2)$$

2.4.2. Analysis of whole blood clotting time

1 mg/mL aggregate solutions were prepared in 0.2 M $CaCl_2$. 25 μL of the obtained solutions were introduced in a siliconized tube, and thermostated at 37 °C for 5 min. Then 0.2 mL fresh ACD blood was introduced. After 0, 20, 40, 60, 80, 100 and 120 min, the tube was gently washed with 100 mL of distilled water. Similar tests without addition of aggregate solution were carried out on

ordinary and siliconized glasses used as positive and negative control, respectively. The absorbance of mixture solution containing ACD blood and distilled water was set as 100. The blood clotting index (BCI) was calculated from the ratio of the absorbance of the samples to that of mixture solution mentioned above. The whole blood clotting time was acquired from the BCI versus time plots (Zhang et al., 2018a,b).

2.4.3. Protein adsorption assay

The amount of proteins adsorbed on the surface of aggregates was studied using the following procedure. Bovine serum albumin (BSA) solution was prepared at 2 mg/mL in PBS. Aggregate solutions at 1 mg/mL were pre-heated in a glass tube at 37 °C, and then mixed with BSA solution. After predetermined time intervals, 1 mL solution was removed and replaced with 1 mL fresh BSA solution. The supernatant was quantified using the Enhanced Bicinchoninic Acid Protein Assay Kit from Beyotime Institute of Biotechnology (Shen et al., 2015). Extracts of ePTFE obtained at 37 °C for 72 h in PBS were used as negative control as recommended by ISO 10993.

2.5. Effect of aggregates on Zebrafish embryo's development

Zebrafish were raised in chlorine-free fish water (FW) under conditions of 10 h dark/14 h light photoperiod at 28.5 °C. The embryos were obtained and transferred to culture dishes containing 25 mL FW with 50 μL of pronase at 50 mg/mL. After 5 min, the FW was replaced with E3 embryos culture medium at pH 7.2. After 4–5 h, the viable embryos were transferred to 96-wells plates and incubated with aggregate solutions (0.05, 0.1, 0.2, 0.5 and 1 mg/mL) at 6–72 hpf (Yostawonkul et al., 2017). Embryos incubated with E3 medium were used as negative control, and E3 medium with acetone as positive control. At the same time, embryos with intact chorionic membranes reared in E3 medium were cultured to indicate the intrinsic embryos quality. The morphological malformation and mortality rate were assessed at 96 hpf (Truong et al., 2012; Pu et al., 2016).

2.6. In vitro drug release

Dialysis method was used to prepare single-loaded and dual-loaded PEG-PLA-PEG aggregates, using hydrophobic PTX and hydrophilic CDDP as model drugs (Jelonek et al., 2015; Jelonek et al., 2016). Briefly, PEG-PLA-PEG copolymer, PTX, and/or CDDP were dissolved in 1 mL of dimethyl formamide (DMF), a water miscible and low toxic solvent. The solution was added into a pretreated dialysis membrane (MWCO = 3500) and dialyzed in PBS containing 0.1% tween during 24 h to obtain single or dual drug loaded aggregates. Drug release was conducted under constant shaking at 37 °C in 40 mL PBS containing 0.1% tween. The whole release medium was renewed at predetermined time intervals (Li et al., 2018).

The amount of PTX was determined using high performance liquid chromatography (HPLC; Shimadzu LC-10A) with a Dionex C18 column and UV detector. The mobile phase was acetonitrile/water mixture with 55/45 vol ratio at a flow rate of 1.0 mL/min. Measurements were made at 227 nm. Meanwhile, CDDP was determined by inductively coupled plasma-atomic emission spectroscopy (ICP-AES; Leeman Prodigy XP).

2.7. Cellular uptake and inhibition of nanotubes

The cellular uptake of nanotubes was measured by using fluorescence microscopy. Dibenzo[a,c][1,2,5]thiadiazolo[3,4-i]phenazine ring derivative (DBTP) with aggregation enhanced near infrared emission (AEE) effect was encapsulated in nanotubes using the same drug loading method described above. Human lung carcinoma cells (A549) were incubated 24 h in 96-well plates. Then, the medium was removed, and 80 μL DBTP loaded nanotubes and 120 μL medium were added. After 8 h incubation, the cells were washed three times with PBS and observed by using optical and fluorescence microscope with BP480-55C excitation module.

The inhibition effect of PTX and CDDP dual-loaded PEG-PLA-PEG nanotubes was investigated by MTT test in comparison with blank, PTX single-loaded, CDDP single-loaded nanotubes and free drugs combination, i.e. mixture of PTX and CDDP with equal amounts. A549 cells were seeded 24 h in 96-well plates, then the culture medium was replaced with 100 μL mixture of fresh medium and samples including blank, PTX single-loaded, CDDP single-loaded, PTX/CDDP dual-loaded nanotubes and free drugs combination at 0.025, 0.25, 2.5, 25 or 50 μg/mL. Fresh medium was used as negative control. Cell viability was obtained through MTT assay as previously described.

2.8. Statistics analysis

Statistics analysis was carried out using SPSS. Descriptive data were represented as arithmetic mean plus or minus standard deviation. Values of $p > 0.05$ were considered not significant, $p < 0.05$ statistically significant, $p < 0.01$ very significant, and $p < 0.001$ extremely significant.

3. Results

3.1. Morphology of self-assembled aggregates

PEG-PLA and PEG-PLGA diblock copolymers were synthesized by ring opening polymerization, and asymmetric PEG-PLA-PEG triblock copolymer was synthesized by combination of ring opening polymerization, chain end functionalization and copper catalyzed click chemistry (Wu et al., 2013; Shen et al., 2017; Liu et al., 2018a,b). The copolymers are abbreviated as EO_xLA_y, $EO_x(LA_yGA_z)$ and $EO_xLA_yEO_{x'}$, where $x(x')$, y, and z represent the number average degree of polymerization (DP) of ethylene oxide, lactyl and glycolyl moieties, respectively.

^{1}H NMR was employed to identify the structure of the different copolymers (Fig. S1). The molar mass and dispersity of the copolymers were obtained by GPC. Table 1 summarizes the characteristics of PEG-PLA, PEG-PLGA and PEG-PLA-PEG block copolymers. The number average molar mass (M_n) of the copolymers ranges from 12,300 for PEG-PLA, 13,400 for PEG-PLGA to 10,900 for PEG-PLA-PEG, and the dispersity ($Đ = M_w/M_n$) from 1.15 to 1.39. The weight fraction of EO moieties (f_{EO}) in PEG-PLA, PEG-PLGA and PEG-PLA-PEG block copolymers is 0.59, 0.43 and 0.72, respectively.

Polymeric aggregates were prepared using co-solvent evaporation from copolymers. Fig. 1 shows the morphology of the various aggregates. Spherical micelles and filomicelles were obtained for PEG-PLGA and PEG-PLA diblock copolymers, respectively (Fig. 1A and B). In contrast, nanotubes were observed in the PEG-PLA-PEG block copolymer (Fig. 1C). The length and diameter of PEG-PLA filomicelles are about 1 μm and 10 nm, respectively, whereas those of PEG-PLA-PEG nanotubes are about 100 nm and 10 nm. Meanwhile, the diameter of PEG-PLGA spherical micelles is in the range of 20–50 nm, which is lower than the value of 114.6 ± 11.7 nm obtained by DLS. The difference could be ascribed to the fact that TEM determines the dehydrated diameter of micelles, whereas DLS measures the hydrodynamic diameter.

The structure of micelles from PEG-PLA diblock copolymers mainly depends upon the hydrophilic to hydrophobic balance (Ahmed and Discher, 2004; Ahmed et al., 2006). In this work, filomicelles were obtained for PEG-PLA with $f_{EO} = 0.59$, which is

Table 1
Characteristics of PEG-PLA, PEG-PLGA and PEG-PLA-PEG block copolymers.

Polymer	EO/LA/GA[a]	DP_{PEG}	DP_{PLA}	DP_{PGA}	M_n[c]	$Đ$[c]	f_{EO}
$EO_{113}LA_{48}$	2.35/1/-	113	48	–	12,300	1.19	0.59
$EO_{113}(LA_{66}GA_{31})$	3.70/2.17/1	113	66	31	13,400	1.39	0.43
$EO_{113}LA_{30}EO_{12}$	4.09/1/-	113, 12[b]	30	–	10,900	1.15	0.72

[a] Calculated from ^{1}H NMR in $CDCl_3$.
[b] DP of the shorter PEG block in the copolymer.
[c] Determined by GPC.

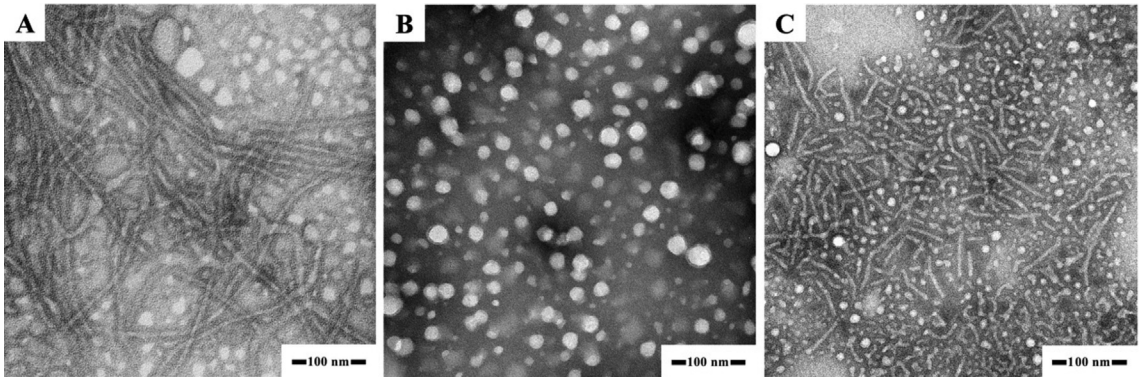

Fig. 1. TEM of filomicelles (A), spherical micelles (B), and nanotubes (C) prepared from $EO_{113}LA_{48}$, $EO_{113}(LA_{66}GA_{31})$ and $EO_{113}LA_{30}EO_{12}$ copolymers.

consistent with previous literature (Wu et al., 2011). In contrast, only spherical micelles were observed for PEG-PLGA with f_{EO} = 0.43, in agreement with our previous work (Liu et al., 2018a). In fact, micelle morphology is also dependent on the regularity of hydrophobic block. Stereoregular PLA blocks seem to favor formation of filomicelles, because PLA are more rigid than PLGA with randomly distributed LA and GA moieties. Concerning PEG-PLA-PEG, the asymmetric chain structure tends to self-assemble hollow structure aggregates in which the longer PEG outside and shorter ones inside because the asymmetry affects the mobility of copolymer chain segments in the self-assembly process (Wu et al., 2013).

3.2. Cytocompatibility of aggregates

3.2.1. Agar diffusion assay

Agar diffusion assay was measured by means of L-929 mouse fibroblast to evaluate the lysosomes' membrane integrity because neutral red preferentially combines to acid regions of cells (Sriram et al., 2011). The cytotoxicity of samples is closely related to the morphological evidences of cell damage such as degeneration, deformation or shedding within the zone (zone index). A zone index of 0 stands for no detectable zone around the sample, 1 for zone limited to region around the sample, 2 for area extending less than 5 mm beyond the sample, 3 for area extending 5–10 mm, 4 for area extending more than 10 mm without relating the whole dish, and 5 for zone involving the entire dish. On the other hand, lysis index is introduced to assess the area of decolorization resulted from injured unstained cells. A lysis index of 0 stands for no cytotoxicity, 1 for less than 20% of area affected, 2 for 20% to 39%, 3 for 40% to 59%, 4 for 60% to 80%, and 5 for more than 80% (Muzzarelli et al., 2005). Furthermore, the response index (the ratio of zone index to lysis index) is used to assess the cytotoxicity: a response index of 0/0–0.5/0.5 stands for none cytotoxicity, 1/1–1.5/1.5 for mild cytotoxicity, 2/2–3/3 for moderate cytotoxicity, and >4/4 for marked cytotoxicity.

There was no decolorization around the test samples after agar diffusion, and L-929 didn't present any sign of cell injury similar to the negative sample (Fig. 2). No signs of cell toxicity were detected around the test samples. In contrast, an area of degradation around the positive sample was detected, and only a few cells survived. Thus the response index of the $EO_{113}LA_{48}$, $EO_{113}(LA_{66}GA_{31})$, $EO_{113}LA_{30}EO_{12}$ aggregates and the negative control was all estimated to be 0/0 as there was no cytotoxicity. And the response index was estimated to be 3/3 for the positive control, in agreement with moderate cytotoxicity. These findings suggest that the aggregates of PEG-PLA, PEG-PLGA and PEG-PLA-PEG block copolymers can be safely used *in vivo* with no detectable cytotoxicity.

3.2.2. MTT test

In vitro cytotoxicity is usually performed by means of MTT test to limit the use of laboratory animals (Sun et al., 2014; Hu et al., 2014). The influence of various aggregates on L-929 mouse fibroblasts and HUVEC is displayed in Fig. 3 and Fig. 4. The viability of cells is well above 75% for all samples even at the highest sample concentration at 1 mg/mL and with the longest incubation time. A slight decrease of the viability is observed for both cell lines ($p > 0.05$) with the increase of sample concentration. Therefore, the different aggregates prepared from PEG-PLA, PEG-PLGA and PEG-PLA-PEG copolymers are not toxic to both L-929 mouse fibroblasts and HUVEC, and can be safely used by intravenous injection. It is also noticed that the viability of both cells is extremely low in the positive group.

3.2.3. Inflammatory cytokine release

Inflammation has an important effect on the development of cancers (He et al., 2015). Macrophages and cytokines are considered as a crucial factor in the process of inflammatory response. The production of IL-1β, TGF-β1 and TNF-α cytokines was determined after culture with the aggregate solutions.

The different aggregates in contact with macrophages derived from THP-1 all affected the release of cytokines including IL-1β, TGF-β1 and TNF-α (Fig. 5), but the influence was extremely low compared to that of the positive group ($p < 0.001$). The concentration of released cytokines IL-1β, TGF-β1 and TNF-α in the presence

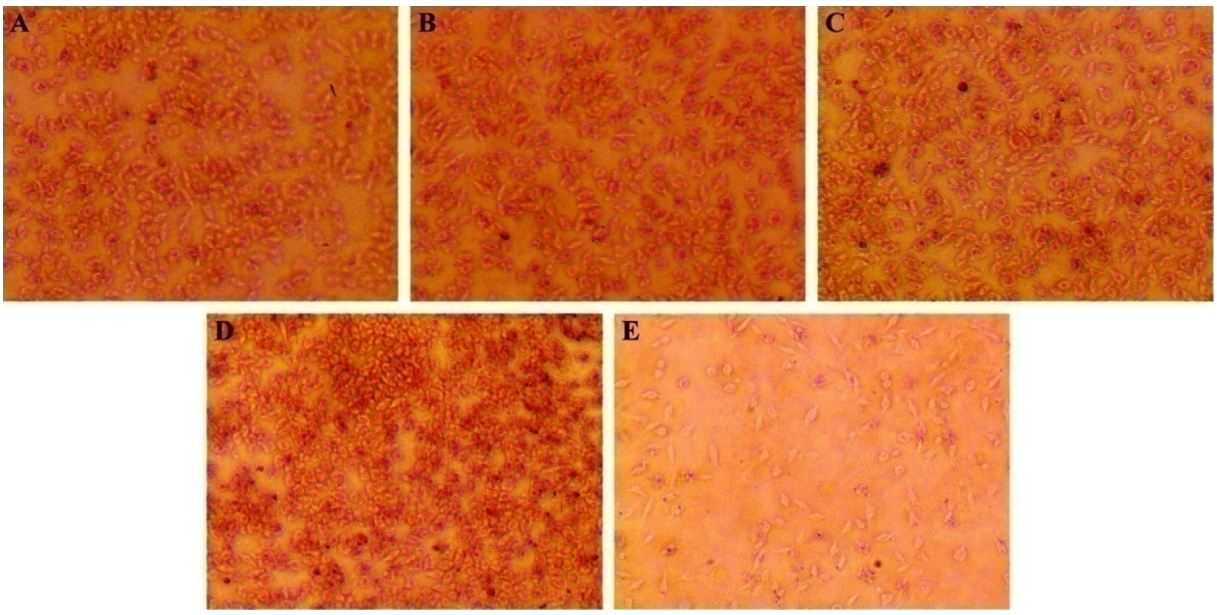

Fig. 2. Microscopic images of L-929 mouse fibroblasts after 24 h exposure to aggregates of $EO_{113}LA_{48}$ (A), $EO_{113}(LA_{66}GA_{31})$ (B), $EO_{113}LA_{30}EO_{12}$ (C), negative control (D), and positive control (E) in agar diffusion test (Magnification = 40×).

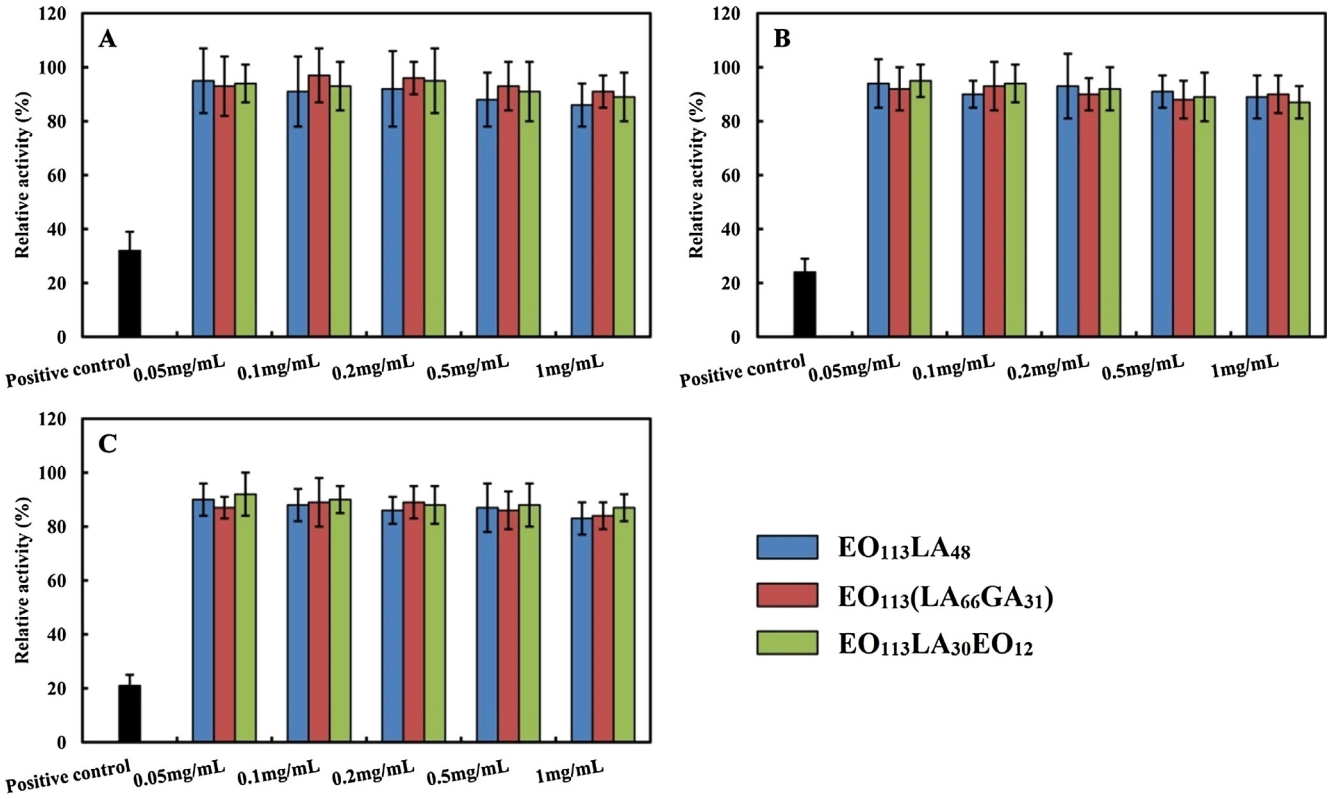

Fig. 3. Relative activity of L-929 mouse fibroblasts after culturing 24 h (A), 48 h (B) and 72 h (C) with aggregates of $EO_{113}LA_{48}$, $EO_{113}(LA_{66}GA_{31})$ and $EO_{113}LA_{30}EO_{12}$ copolymers.

of PEG-PLA filomicelles was 212, 29 and 25 pg/mL, respectively. Similarly, the concentration of released cytokines IL-1β, TGF-β1 and TNF-α was 216, 30, 23 pg/mL for PEG-PLGA spherical micelles, and 203, 24, 20 pg/mL for PEG-PLA-PEG nanotubes. $EO_{113}(LA_{66}GA_{31})$ and $EO_{113}LA_{48}$ stimulated slightly higher cytokine release than $EO_{113}LA_{30}EO_{12}$. It is noteworthy that the release of cytokines is at the equivalent level for $EO_{113}LA_{30}EO_{12}$ and the negative group in most cases ($p > 0.05$). Therefore, it is concluded that the effect of PEG-PLA, PEG-PLGA and PEG-PLA-PEG aggregates on cytokine secretion is significantly low in comparison with the positive group, indicating that they would not cause serious inflammatory activity (Feliu et al., 2012; Fuchs et al., 2016). These results further evidence the excellent cytocompatibility of PEG-PLA, PEG-PLGA and PEG-PLA-PEG copolymer aggregates.

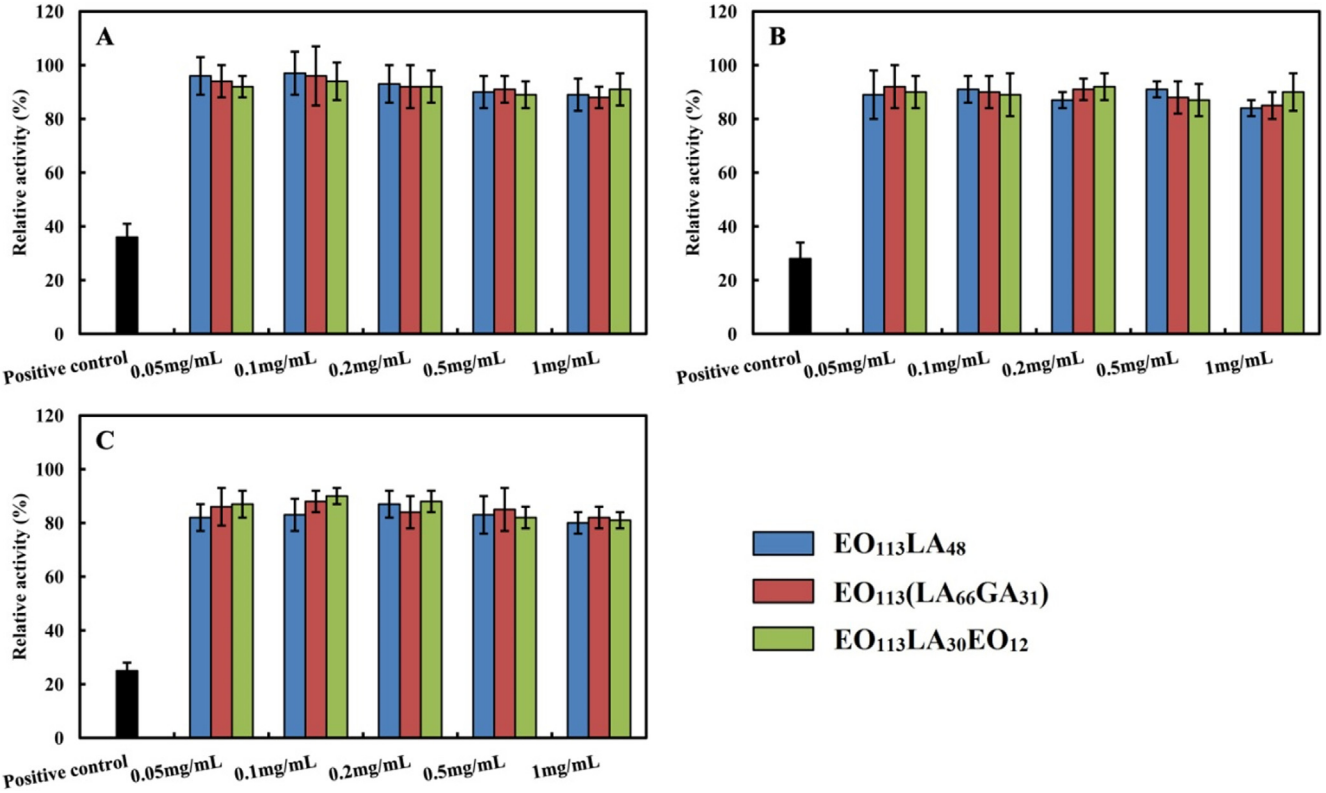

Fig. 4. Relative activity of HUVEC cells after culturing 24 h (A), 48 h (B) and 72 h (C) with aggregates of $EO_{113}LA_{48}$, $EO_{113}(LA_{66}GA_{31})$ and $EO_{113}LA_{30}EO_{12}$ copolymers.

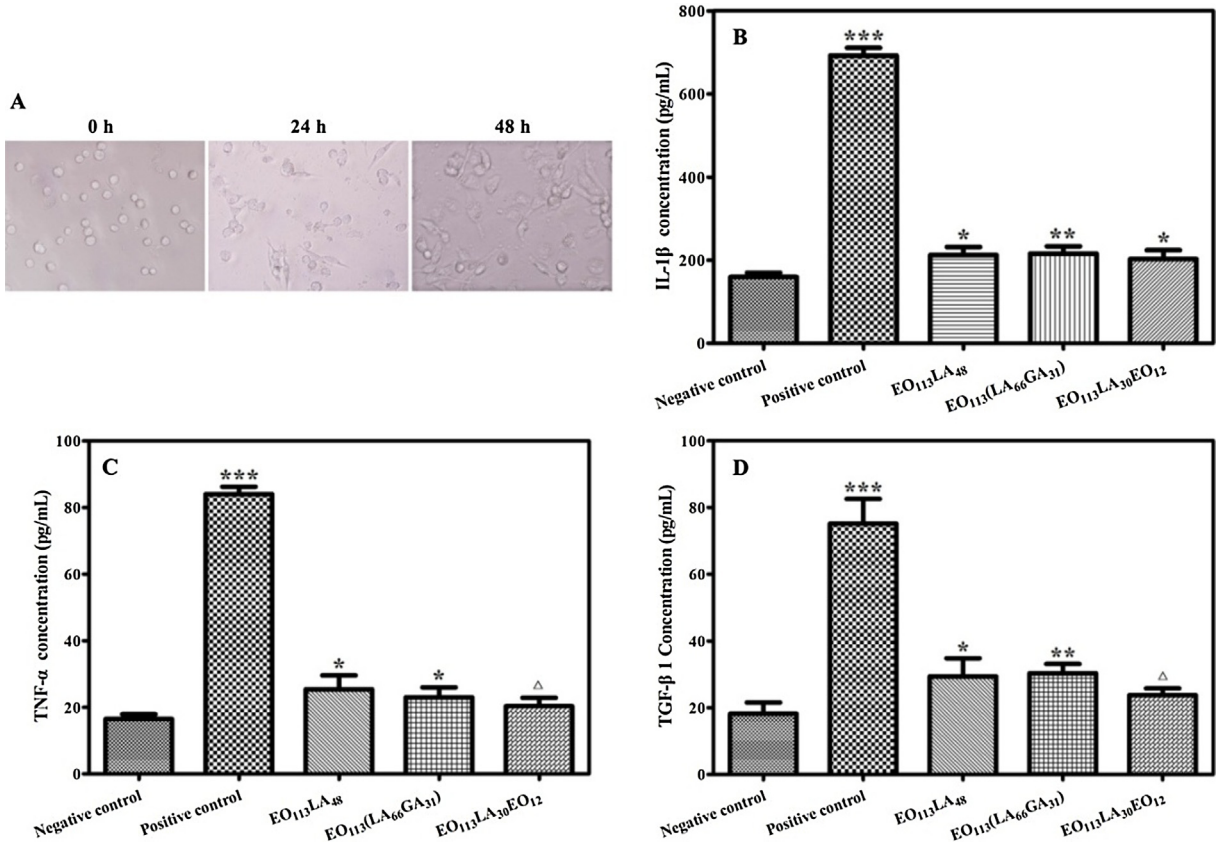

Fig. 5. Differentiation process of adherent macrophages from suspension THP-1 induced by PMA stimulation (A). Release profile of IL-1β (B), TNF-α (C) and TGF-β1 (D) by macrophages derived from THP-1 after contact with PEG-PLA, PEG-PLGA, PEG-PLA-PEG aggregates, negative group and positive group. △ represented $p > 0.05$, * $p < 0.05$, ** $p < 0.01$, and *** $p < 0.001$ versus negative control.

3.3. Hemocompatibility of aggregates

3.3.1. Hemolysis test

Hemolysis test is widely used to determine the hemolytic ratio (HR) which reflects the influence of medical materials on red blood cell (RBC). The value of HR indicates the level of hemoglobin dissociation and hemolysis after aggregates are co-cultured with RBC *in vitro*. Lower HR indicates lower breaking level of RBC (Xiong et al., 2016a,b).

When the value of HR is below 5%, the blood hemolytic properties are generally acceptable (Yang et al., 2010). Table 2 displays the HR data of the various aggregates together with those of the controls. The HR value of $EO_{113}LA_{48}$, $EO_{113}(LA_{66}GA_{31})$ and $EO_{113}LA_{30}EO_{12}$ aggregates is 2.9%, 3.7% and 2.2%, respectively. Considering that the OD values of both positive and negative groups are within the suggested range of ISO 10993, the HR values of aggregates prepared from PEG-PLA, PEG-PLGA and PEG-PLA-PEG are all below 5%, suggesting excellent hemocompatibility.

3.3.2. Quantification of whole blood clotting time

The whole blood clotting time test is generally employed to evaluate the effect of materials on the occurrence of intrinsic coagulation. Actually, it allows to assess the activation level of intrinsic coagulation (Khatun et al., 2015). Endogenous blood clotting turns up when aggregates are exposed to blood, and the level of blood clotting increases as the exposure time increases.

The whole blood clotting of aggregates prepared from PEG-PLA, PEG-PLGA and PEG-PLA-PEG copolymers was obtained from the changes of BCI values over time as displayed in Fig. 6. The absorbance reaching 0.1 or 0.01 is generally regarded as the initial clotting and the whole clotting time, respectively. The slower the decrease in BCI value, the longer the coagulation time. Test samples and the negative control present similar BCI changes with a whole clotting time of about 50 min. The positive control exhibits much quicker decrease in BCI and the whole clotting time was 20 min. The results show that PEG-PLA, PEG-PLGA and PEG-PLA-PEG aggregates would not interplay with fibrinogen which has important effect on coagulation process in the blood.

3.3.3. Protein adsorption assay

When aggregates are exposed to blood, the first thing is plasma proteins adsorption on the surface (Jiang et al., 2015). Using ePTFE extracts as negative control, PEG-PLA, PEG-PLGA and PEG-PLA-PEG aggregates were incubated in BSA solution to determine protein adsorption. The amount of adsorbed protein (μg) per mg of aggregates was calculated by using gravimetry.

Fig. 7 exhibits the adsorption process of BSA on the aggregates of copolymers. The adsorption rate of all samples is very fast in the first 10 min, and then levels off. Interestingly, the amount of adsorbed protein slightly decreases at the last stages, which could be related to the operation of BSA solution renewal. The amount of adsorbed protein on aggregates is higher than that of the negative control at all time points, but the increase is rather limited. Considering the overall results of hemolysis, whole blood clotting time and protein adsorption, it is concluded that the aggregates present good hemocompatibility.

Table 2
Hemolysis ratio (%) of $EO_{113}LA_{48}$, $EO_{113}(LA_{66}GA_{31})$ and $EO_{113}LA_{30}EO_{12}$ aggregates.

Sample	OD value	Hemolysis ratio (%)
H_2O	0.913 ± 0.065	Positive group
Saline	0.025 ± 0.007	Negative group
$EO_{113}LA_{48}$	0.051 ± 0.007	2.9 ± 0.8
$EO_{113}(LA_{66}GA_{31})$	0.058 ± 0.004	3.7 ± 0.5
$EO_{113}LA_{30}EO_{12}$	0.045 ± 0.009	2.2 ± 1.0

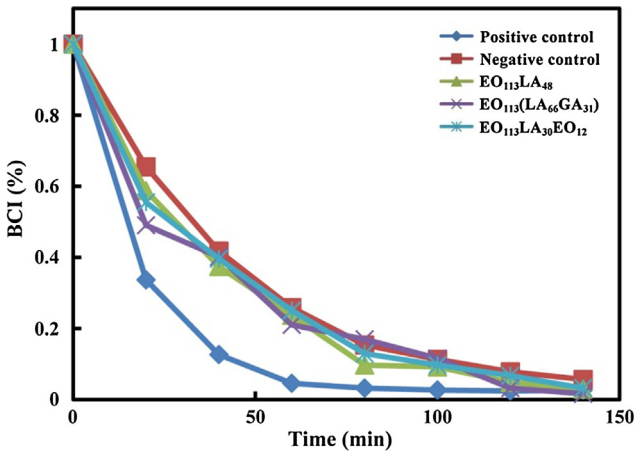

Fig. 6. Blood clotting index changes as a function of time for $EO_{113}LA_{48}$, $EO_{113}(LA_{66}GA_{31})$ and $EO_{113}LA_{30}EO_{12}$ aggregates in comparison with the controls.

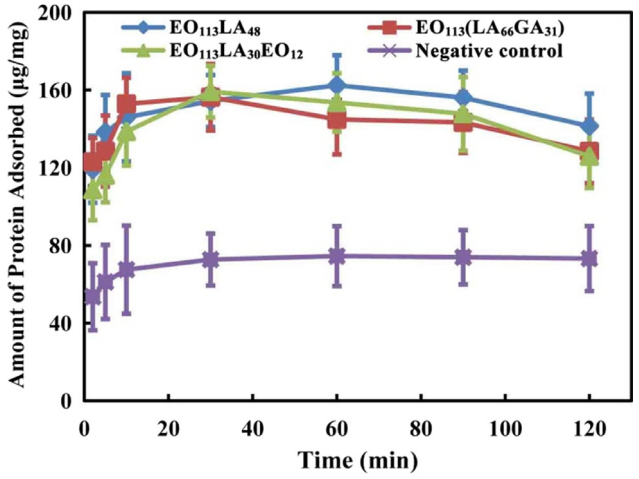

Fig. 7. Protein adsorption on $EO_{113}LA_{48}$, $EO_{113}(LA_{66}GA_{31})$ and $EO_{113}LA_{30}EO_{12}$ aggregates in BSA solution at 2 mg/mL.

3.4. Effect of aggregates on Zebrafish embryo's development

Zebrafish are increasingly used as vertebrate model to evaluate the safety and toxicity of drugs *in vivo* (Webster et al., 2016). Many studies have demonstrated that Zebrafish and mammals have similar responses to materials (Chang et al., 2016; Fenaroli et al., 2014; Liu et al., 2013). Toxicity and safety evaluations of Zebrafish have also been accepted by the USA FDA and European Agency for the Evaluation of Medicinal Products (EMEA) (Zhu et al., 2018; He et al., 2014; Hill et al., 2012). Therefore, the embryonic development of Zebrafish is a means to evaluate the *in vivo* biocompatibility of aggregates.

The mortality and malformation rates of Zebrafish embryos co-cultured with PEG-PLA, PEG-PLGA and PEG-PLA-PEG aggregates are shown in Fig. 8 and Table 3. At a concentration of 0.05 mg/mL, the mortality rates of embryos are all below 1%, and no malformation is observed. At concentrations of 0.1 and 0.2 mg/mL, the mortality rates are around 1% without any malformation. At 0.5 mg/mL, the mortality rates are below 2%. But the total malformation rate increases to 4.2%, 6.7% and 4.1% for $EO_{113}LA_{48}$, $EO_{113}(LA_{66}GA_{31})$ and $EO_{113}LA_{30}EO_{12}$, respectively. The malformation is mainly single deformation. At 1.0 mg/mL, higher mortality and malformation rates are obtained, ranging from 3.9% to 5.2%, and from 10.3% to 15.6%, respectively. Obvious increase of embryos with

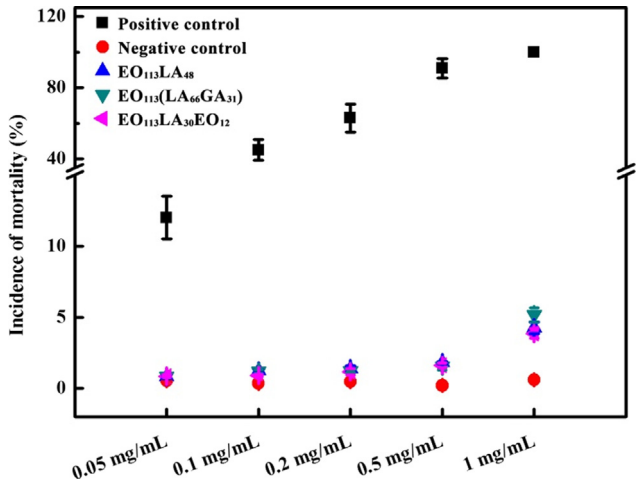

Fig. 8. Mortality rates of Zebrafish embryos exposed to $EO_{113}LA_{48}$, $EO_{113}(LA_{66}GA_{31})$ and $EO_{113}LA_{30}EO_{12}$ aggregates at different concentrations during 6–72 hpf.

multi-malformations is also noticed (Fig. 9), including yolk sac edema, caudal fin abnormal, bent body axis, pericardial edema, yolk sac opaque, yolk sac absorption delay, and composite deformities. The three aggregate solutions at 1 mg/mL could induce almost all types of malformation in Zebrafish embryos mentioned above.

In the case of the positive control (acetone), the mortality rate is 100% at 1.0 mg/mL. At 0.5 mg/mL, the mortality rate decreases to 91%, and the malformations rate is 18.4% with multi-malformations. With decreasing concentration, the acetone's impact on mortality and malformation of embryos also becomes weaker. Therefore, it can be concluded that the aggregates formed of PEG-PLA, PEG-PLGA and PEG-PLA-PEG copolymers present good biocompatibility *in vivo*.

3.5. In vitro drug release

$EO_{113}LA_{30}EO_{12}$ nanotubes were loaded with PTX and/or CDDP to evaluate their potential as novel carrier of single or dual-loaded drugs. The encapsulation efficiency (EE) is stated as the ratio of the amount of encapsulated drug to that of initially introduced drug, and the drug loading content (LC) as the ratio of the amount of encapsulated drug to the total amount of drug encapsulated nanotubes (Liu et al., 2018a,b). As displayed in Table 4, the EE of PTX and CDDP single-loaded nanotubes is 78.9 ± 6.2% and 79.8 ± 7.6%, respectively, whereas the EE of PTX and CDDP dual-loaded nanotubes were 63.1 ± 8.1% and 70.5 ± 5.7%.

The *in vitro* drug release of single- or dual-loaded nanotubes was comparatively studied as shown in Fig. 10. The accumulated amount of released PTX rapidly increases in the first 20 days to reach nearly 37% for single-loaded nanotubes. Beyond, the increase slows down, and the amount of released PTX reaches 41% in 120 days. The release of CDDP is much slower from single-loaded nanotubes. Only 15% of CDDP is released in the 120 days period. It is noteworthy that the release medium contains NaCl and KCl, which could ensure the stability of CDDP during the drug release period. These results indicate that PEG-PLA-PEG nanotubes could be very promising for co-delivery of compounds with different water solubility. In contrast, drug release is slower from dual-loaded nanotubes. Nearly 33% of PTX and 12% of CDDP were released in 120 days.

3.6. Cellular uptake and inhibition of nanotubes

Drug-loaded polymeric nano-carriers have longer circulation time *in vivo* than free drug, thereby improving uptake of drugs by tumor tissue. The ability of entering tumor cells is important in maximizing the function of PTX/CDDP dual-loaded nanotubes, and is also the key to success of drug delivery systems.

Table 3
Malformation rate of Zebrafish embryos exposed to $EO_{113}LA_{48}$, $EO_{113}(LA_{66}GA_{31})$ and $EO_{113}LA_{30}EO_{12}$ aggregates at different concentrations during 6–72 hpf.

Sample	Total malformation rate (%)				
	1.0 mg/mL	0.5 mg/mL	0.2 mg/mL	0.1 mg/mL	0.05 mg/mL
$EO_{113}LA_{48}$	12.6 ± 4.9	4.2 ± 2.6	0	0	0
$EO_{113}(LA_{66}GA_{31})$	15.6 ± 5.8	6.7 ± 3.5	0	0	0
$EO_{113}LA_{30}EO_{12}$	10.3 ± 4.2	4.1 ± 1.8	0	0	0
Positive control	–	18.4 ± 7.9	11.3 ± 4.0	6.3 ± 3.5	0
Negative control	0	0	0	0	0

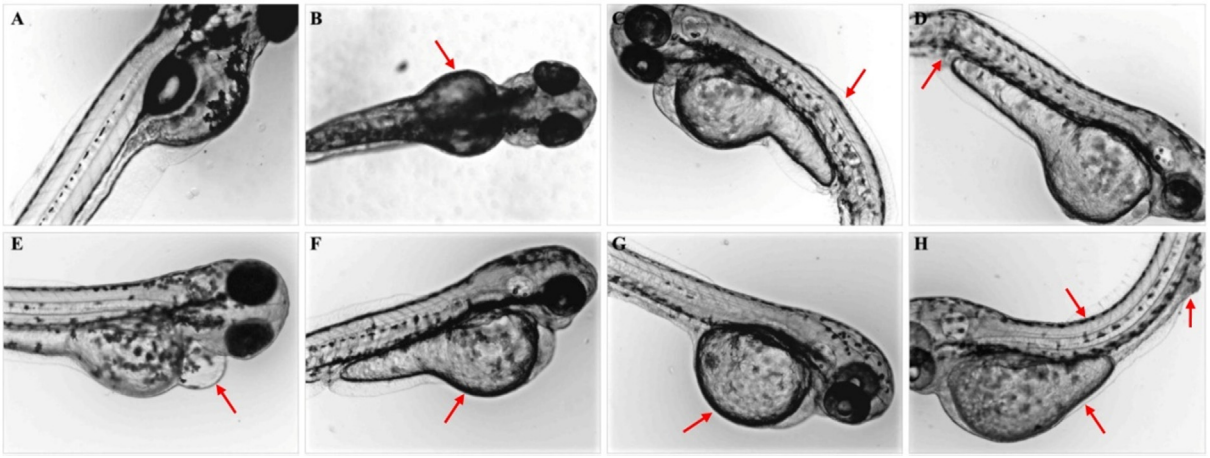

Fig. 9. Types of aggregate-induced malformation in Zebrafish embryos at 96 hpf: (A) normal development; (B) yolk sac edema; (C) bent body axis; (D) caudal fin abnormal; (E) pericardial edema; (F) yolk sac absorption delay; (G) yolk sac opaque; (H) composite deformities.

Table 4
Encapsulation efficiency and drug loading in single- and dual-loaded nanotubes.

Drug in nanotubes	EE (%)	LC (%)
PTX single-loaded	78.9 ± 6.2	7.3 ± 0.5
CDDP single-loaded	79.8 ± 7.6	7.4 ± 0.7
PTX dual-loaded	63.1 ± 8.1	5.9 ± 0.7
CDDP dual-loaded	70.5 ± 5.7	6.6 ± 0.5

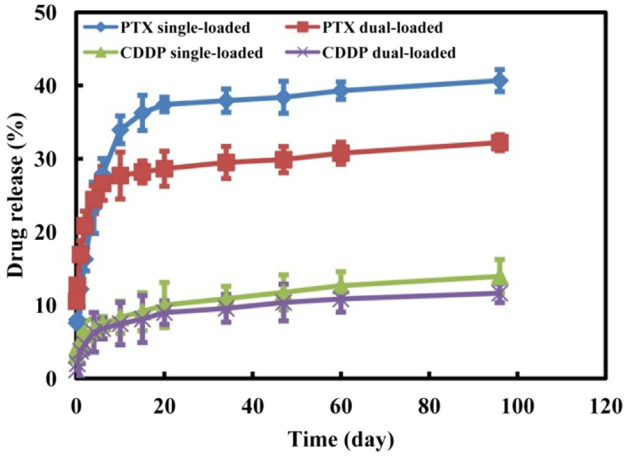

Fig. 10. In vitro cumulative drug release of PTX and CDDP single- and dual-loaded nanotubes.

DBTP-encapsulated nanotubes were incubated with A549 cells for 8 h at 37 °C. As shown in Fig. 11A, A549 grows well in the cell plate, but the cell density is only about 30%. Fig. 11B shows the same field of view under fluorescence microscope in which red fluorescence emitted by DBTP can be observed. A549 cells are observed in the same position with DBTP showing a state of positional coincidence. There is practically no red fluorescence in areas without cells, indicating that most of the DBTP-encapsulated nanotubes were taken up by cells.

MTT test was used to determine the influence of free drugs combination, PTX single-load, CDDP single-loaded, and PTX/CDDP dual-loaded nanotubes on A549 after 72 h co-culture. As shown in Fig. 12, the A549 relative proliferation rate of free drugs is the lowest in all concentrations from 0.025 to 50 μg/mL, indicating that free drugs present the highest cytotoxicity. Cells co-cultured with PTX/CDDP dual-loaded nanotubes exhibit lower rates than treatments with PTX single-load and CDDP single-loaded nanotubes.

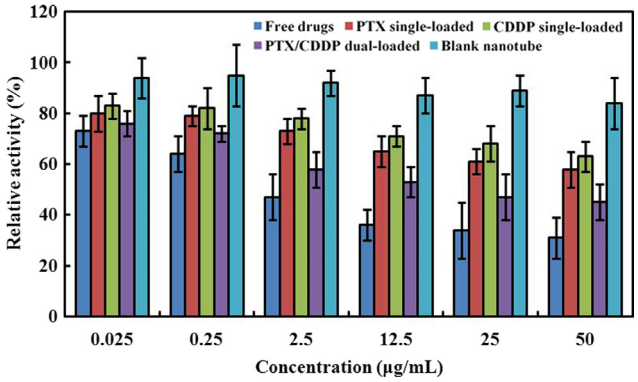

Fig. 12. Relative activity (%) of A549 cells after 72 h exposure to free drugs combination, PTX single-loaded nanotubes, CDDP single-loaded nanotubes, PTX/CDDP dual-loaded nanotubes and blank nanotubes at various concentrations.

Meanwhile, the highest relative growth rates of A549 are observed for blank nanotubes, which also evidenced the good biocompatibility and biosafety of nanotubes. In addition, with increasing concentration of PTX and CDDP free drugs, the relative growth rates of A549 tend to decrease, in agreement with the high anti-cancer cell activity of free drugs. The same trend is observed for PTX single-loaded, CDDP single-loaded, or PTX/CDDP dual-loaded nanotubes, dual-loaded nanotubes showing better therapeutic effect on tumor cells than single-loaded ones.

4. Discussion

The development of combination therapy with distinct functional drugs requires drug carrier with characteristics in terms of biocompatibility, drug loading, co-delivery, etc. (Doppalapudi et al., 2016; Karimi et al., 2016).

Biocompatibility of PEG-PLA, PEG-PLGA and PEG-PLA-PEG aggregates was assessed in terms of cell compatibility, blood compatibility *in vitro* and Zebrafish embryonic compatibility *in vivo*. L-929 mouse fibroblast is a standard cell line commonly used in cell compatibility assessment (Jung et al., 2015). Vascular endothelial cells are also of interest as the aggregates are nano drug carrier administered by intravenous injection. Once in the blood circulation, the aggregates will be first in contact with vascular endothelial cells. Thus both L-929 mouse fibroblasts and HUVEC were employed in MTT test (Figs. 4 and 5). The results show that the aggregates are not toxic to both L-929 and HUVEC. Moreover, the difference in the viability between both cell lines is not statistically

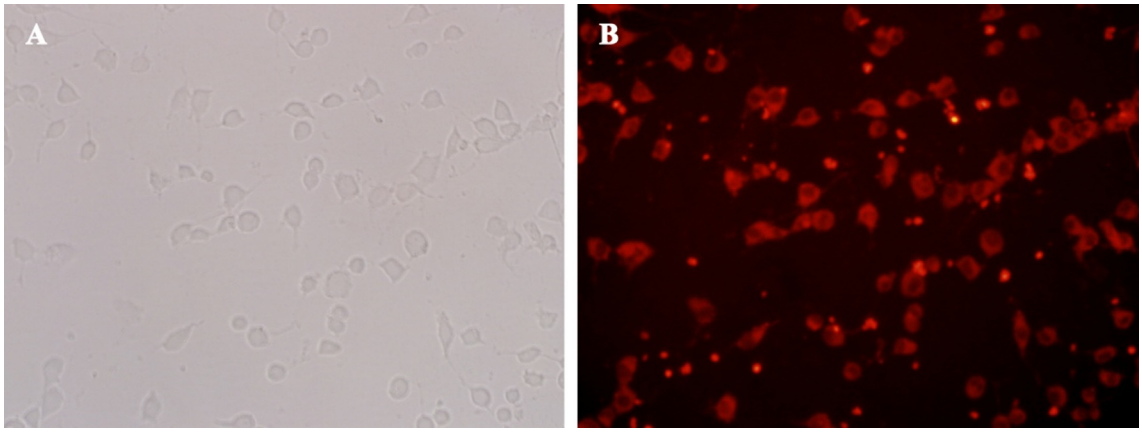

Fig. 11. Images of A549 cells after co-culture with nanotubes containing DBTP at 37 °C for 8 h using light microscopy (A) and fluorescence microscopy (B), (Magnification = 40×).

significant. Agar diffusion test was carried out to assess the cell toxicity using L-929 mouse fibroblasts only (Fig. 3). The results are consistent with our previous results on PEG-PLA filomicelles and PEG-PLGA spherical micelles (Liu et al., 2018a,b; Shen et al., 2017).

Hemolysis is a phenomenon in which RBC break open, causing hemoglobin release into the surrounding environment (Kim et al., 2005). Hemolysis test indicates that PEG-PLA-PEG nanotubes induce the lowest breaking open degree of RBC, whereas PEG-PLA spherical micelles cause the highest (Table2). Broken RBC can lead to coagulation (Xiong et al., 2016a,b). Nanotubes and spherical micelles also lead to the lowest and highest degrees of coagulation in the quantification of whole blood clotting time at 60 min of contact between aggregates and ACD blood (Fig. 7). Meanwhile, the adsorption amount of BSA on nanotubes in the first 30 min of the protein adsorption assay is the lowest, whereas that of spherical micelles is the highest. This finding is consistent with the fact that protein adsorption is responsible for triggering hemolysis (Jiang et al., 2015). The same trend is also detected in the effects of aggregates on inflammatory cytokine release and Zebrafish embryo's development (Fig. 6 and Table3).

Few studies have been reported on the drug encapsulation and release profiles of single and multi-loaded drug delivery systems (Wang et al., 2011; Li et al., 2016). In this work, single and dual-loading of hydrophilic CDDP and hydrophobic PTX are realized in the nanotubes with the presence of a hydrophilic core, a hydrophobic middle layer and a hydrophilic corona. The results confirm that nanotubes formed of PEG-PLA-PEG copolymer are efficient for co-delivery of both hydrophobic and hydrophilic agents (Fig. 11). The EE values of single-loaded nanotubes are obviously higher than those of dual-loaded ones for both PTX and CDDP. Similarly, the LC values of single-loaded nanotubes are slightly higher than those of dual-loaded ones (Table 4). Nevertheless, the total drug amount of dual-loaded nanotubes is higher than that of single-loaded nanotubes. The results of drug release could appear surprising because hydrophilic CDDP is released at a slower rate as compared to PTX. In fact, the difference could be attributed to the location of drugs in the nanotubes' architecture. CDDP could be mainly entrapped in the internal hydrophilic region, and can thus hardly diffuse out through the intermediate hydrophobic layer. On the other hand, the release of both drugs is slower from dual-loaded nanotubes than from single-loaded ones. But the total amount of released drugs in higher for dual-loaded nanotubes than from single-loaded ones. This finding further evidences the potential of nanotubes for co-delivery of agents with different water solubility.

After 8 h co-culturing of DBTP-loaded nanotubes with A549 cells, the number of cells in the plate decreased, probably because DBTP can inhibit cell growth resulting in partial apoptosis of tumor cells. This once again demonstrated that PEG-PLA-PEG triblock copolymer self-assembled nanotubes are capable of delivering entrapped agents into tumor cells Cellular uptake and inhibition results showed that PTX/CDDP dual-loaded nanotubes can be successfully taken in by tumor cells and effectively inhibit cells growth. Although PTX/CDDP dual-loaded nanotubes present slightly lower cytotoxicity than free drugs on tumor cells, they are most promising for applications in cancer combination therapy considering targeting function, long blood circulation, and high drug loading.

5. Conclusions

Self-assembled nanotubes were prepared from PEG-PLA-PEG triblock copolymer by co-solvent evaporation. The biocompatibility of nanotubes was evaluated compared to filomicelles and spherical micelles prepared from EPG-PLA and PEG-PLGA copolymers. Several biocompatibility aspects of aggregates were studied, including agar diffusion and MTT test, cytokines release, dynamic clotting, hemolytic test, protein adsorption *in vitro*, and Zebrafish embryonic compatibility *in vivo*.

The cell viability data obtained from agar diffusion and MTT assay show that all samples have little effect on cell adhesion and proliferation, and slight increase in cytokines release is detected in comparison with the negative control. The various aggregates exhibit low hemolysis ratios, suggesting good hemolytic properties. Low BSA adsorption and little effect on the dynamic clotting were also detected. Moreover, the samples present no toxicity towards the Zebrafish embryos development. Therefore, all the results indicate that the different aggregates, in particular PEG-PLA-PEG nanotubes present outstanding cytocompatibility, hemocompatibility and embryonic compatibility.

Single- and dual-loaded nanotubes were prepared using hydrophobic PTX and hydrophilic CDDP as anti-tumor drugs. High drug load content and encapsulation efficiency were obtained. The release of both drugs was slower from dual-loaded nanotubes than from single-loaded ones. But the total amount of released drugs in higher for dual-loaded nanotubes than from single-loaded ones. Cellular uptake and inhibition results showed that PTX/CDDP dual-loaded nanotubes were successfully taken in by tumor cells and effectively inhibited cell growth.

Taking into account the outstanding biocompatibility, drug loading capacity, dual-loading of both hydrophilic and hydrophobic drugs, cellular uptake and inhibition, it is concluded that the nanotubes obtained from asymmetric PEG-PLA-PEG triblock copolymers are most promising for co-delivery of anti-tumor drugs in combination therapy.

Acknowledgements

This work was sponsored by the Science and Technology Development Plan of Shandong Province (No. 2018GGX102016).

Appendix A. Supplementary material

Supplementary data to this article can be found online at https://doi.org/10.1016/j.jsps.2019.08.005.

References

Ahmed, F., Discher, D.E., 2004. Self-porating polymersomes of PEG-PLA and PEG-PCL: hydrolysis-triggered controlled release vesicles. J. Control. Release 96 (1), 37–53.
Ahmed, F. et al., 2006. Biodegradable polymersomes loaded with both paclitaxel and doxorubicin permeate and shrink tumors, inducing apoptosis in proportion to accumulated drug. J. Control. Release 116 (2), 150–158.
Chang, H. et al., 2016. Predicting the in vivo accumulation of nanoparticles in tumor based on in vitro macrophage uptake and circulation in Zebrafish. J. Control. Release 244, 205–213.
Doppalapudi, S. et al., 2016. Biodegradable polymers for targeted delivery of anti-cancer drugs. Expert Opin. Drug Del. 13 (6), 891–909.
Feliu, N. et al., 2012. Stability and biocompatibility of a library of polyester dendrimers in comparison to polyamidoamine dendrimers. Biomaterials 33 (7), 1970–1981.
Fenaroli, F. et al., 2014. Nanoparticles as drug delivery system against tuberculosis in Zebrafish embryos: direct visualization and treatment. ACS Nano 8 (7), 7014–7026.
Fuchs, A.K. et al., 2016. Carboxyl- and amino-functionalized polystyrene nanoparticles differentially affect the polarization profile of M1 and M2 macrophage subsets. Biomaterials 85, 78–87.
Gao, Y. et al., 2010. Linear cationic click polymer for gene delivery: Synthesis, biocompatibility, and in vitro transfection. Biomacromolecules 11 (11), 3102–3111.
Harada, T., Discher, D.E., 2011. Materials science: Bubble wrap of cell-like aggregates. Nature 471 (7337), 172–173.
He, J.H. et al., 2014. Zebrafish models for assessing developmental and reproductive toxicity. Neurotoxicol. Teratol. 42, 35–42.
He, Z.L. et al., 2015. Degradation and bio-safety evaluation of mPEG-PLGA-PLL copolymer-prepared nanoparticles. J. Phys. Chem. C 119 (6), 3348–3362.

Hill, A. et al., 2012. Comparisons between *in vitro* whole cell imaging and *in vivo* Zebrafish-based approaches for identifying potential human hepatotoxicants earlier in pharmaceutical development. Drug Metab. Rev. 44 (1), 127–140.
Hu, Y. et al., 2014. Thermo-responsive release of curcumin from micelles prepared by self-assembly of amphiphilic P (NIPAAm-co-DMAAm)-b-PLLA-b-P (NIPAAm-co-DMAAm) triblock copolymers. Int. J. Pharmaceut. 476 (1–2), 31–40.
Jelonek, K. et al., 2016. Multidrug PLA-PEG filomicelles for concurrent delivery of anticancer drugs-The influence of drug-drug and drug-polymer interactions on drug loading and release properties. Int. J. Pharmaceut. 510 (1), 365–374.
Jelonek, K. et al., 2015. Self-assembled filomicelles prepared from polylactide/poly (ethylene glycol) block copolymers for anticancer drug delivery. Int. J. Pharmaceut. 485 (1–2), 357–364.
Jiang, L. et al., 2015. Overcoming drug-resistant lung cancer by paclitaxel loaded dual-functional liposomes with mitochondria targeting and pH-response. Biomaterials 52, 126–139.
Jung, O. et al., 2015. Optimized in vitro procedure for assessing the cytocompatibility of magnesium-based biomaterials. Acta Biomater. 23, 354–363.
Karimi, M. et al., 2016. Smart micro/nanoparticles in stimulus-responsive drug/gene delivery systems. Chem. Soc. Rev. 45, 1457–1501.
Khatun, Z. et al., 2015. A hyaluronic acid nanogel for photo-chemo theranostics of lung cancer with simultaneous light-responsive controlled release of doxorubicin. Nanoscale 7 (24), 10680–10689.
Kim, D. et al., 2005. Interaction of PLGA nanoparticles with human blood constituents. Colloids Surf. B Biointerfaces 40 (2), 83–91.
Li, H. et al., 2016a. Cisplatin and doxorubicin dual-loaded mesoporous silica nanoparticles for controlled drug delivery. RSC Adv. 6 (96), 94160–94169.
Li, J. et al., 2018. Tumor-pH-sensitive PLLA-based microsphere with acid cleavable acetal bonds on the backbone for efficient localized chemotherapy. Biomacromolecules 19 (7), 3140–3148.
Li, Z.B. et al., 2016b. Recent advances in stereocomplexation of enantiomeric PLA-based copolymers and applications. Prog. Polym. Sci. 62, 22–72.
Liu, C.W. et al., 2013. Graphene-based anticancer nanosystem and its biosafety evaluation using a Zebrafish model. Biomacromolecules 14 (2), 358–366.
Liu, X. et al., 2018a. Biocompatibility evaluation of self-assembled micelles prepared from poly (lactide-co-glycolide)-poly (ethylene glycol) diblock copolymers. Polym. Adv. Technol. 29 (1), 205–215.
Liu, X. et al., 2018b. Self-assembled filomicelles prepared from polylactide-poly (ethylene glycol) diblock copolymers for sustained delivery of cycloprotoberberine derivatives. Saudi Pharm. J. 26 (3), 342–348.
Loverde, S.M. et al., 2011. Curvature, rigidity, and pattern formation in functional polymer micelles and vesicles-from dynamic visualization to molecular simulation. Curr. Opin. Solid St. M. 15 (6), 277–284.
Lv, S.X. et al., 2014. Co-delivery of doxorubicin and paclitaxel by PEG-polypeptide nanovehicle for the treatment of non-small cell lung cancer. Biomaterials 35 (23), 6118–6129.
Muzzarelli, R.A.A. et al., 2005. The biocompatibility of dibutyryl chitin in the context of wound dressings. Biomaterials 26 (29), 5844–5854.
Pu, Y. et al., 2016. Synthesis and antibacterial study of sulfobetaine/quaternary ammonium-modified star-shaped poly [2-(dimethylamino) ethyl methacrylate]-based copolymers with an inorganic core. Biomacromolecules 18 (1), 44–55.
Shen, X. et al., 2015. In vitro biocompatibility evaluation of bioresorbable copolymers prepared from L-lactide, 1, 3-trimethylene carbonate, and glycolide for cardiovascular applications. J. Biomat. Sci., Polym. E. 26 (8), 497–514.
Shen, X. et al., 2017. Biocompatibility of filomicelles prepared from poly (ethylene glycol)-polylactide diblock copolymers as potential drug carrier. J. Biomat. Sci., Polym. E. 28 (15), 1677–1694.
Sriram, M.I. et al., 2011. Biofilm inhibition and antimicrobial action of lipopeptide biosurfactant produced by heavy metal tolerant strain Bacillus cereus NK1. Colloids Surf. B Biointerfaces 85 (2), 174–181.
Sun, Y. et al., 2014. The strategy to improve gene transfection efficiency and biocompatibility of hyperbranched PAMAM with the cooperation of PEGylated hyperbranched PAMAM. Int. J. Pharmaceut. 465 (1–2), 112–119.
Truong, L. et al., 2012. Media ionic strength impacts embryonic responses to engineered nanoparticle exposure. Nanotoxicology 6 (7), 691–699.
Tyler, B. et al., 2016. Polylactic acid (PLA) controlled delivery carriers for biomedical applications. Adv. Drug Deliver. Rev. 107, 163–175.
Wang, H. et al., 2011. Enhanced anti-tumor efficacy by co-delivery of doxorubicin and paclitaxel with amphiphilic methoxy PEG-PLGA copolymer nanoparticles. Biomaterials 32 (32), 8281–8290.
Wauters, A.C. et al., 2018. Development of morphologically discrete PEG-PDLLA nanotubes for precision nanomedicine. Biomacromolecules 20 (1), 177–183.
Webster, C.A. et al., 2016. An early developmental vertebrate model for nanomaterial safety: bridging cell-based and mammalian toxicity assessment. Nanomedicine 11 (6), 643–656.
Williams, D.F., 2008. On the mechanisms of biocompatibility. Biomaterials 29 (20), 2941–2953.
Wu, X.H., El Ghzaoui, A., Li, S.M., 2011. Anisotropic self-assembling micelles prepared by the direct dissolution of PLA/PEG block copolymers with a high PEG fraction. Langmuir 27 (13), 8000–8008.
Wu, X. et al., 2013. Modeling and self-assembly behavior of PEG-PLA-PEG triblock copolymers in aqueous solution. Nanoscale 5 (19), 9010–9017.
Wu, Z.X. et al., 2014. Thermosensitive hydrogel used in dual drug delivery system with paclitaxel-loaded micelles for in situ treatment of lung cancer. Colloids Surf. B Biointerfaces 122, 90–98.
Xiong, F. et al., 2016a. Superparamagnetic anisotropic nano-assemblies with longer blood circulation *in vivo*: a highly efficient drug delivery carrier for leukemia therapy. Nanoscale 8 (39), 17085–17089.
Xiong, H. et al., 2016b. Mitochondria and nuclei dual-targeted heterogeneous hydroxyapatite nanoparticles for enhancing therapeutic efficacy of doxorubicin. Biomaterials 94, 70–83.
Yang, Y. et al., 2010. A novel electrochemical strategy for improving blood compatibility of titanium-based biomaterials. Colloids Surf. B Biointerfaces 79 (1), 309–313.
Yostawonkul, J. et al., 2017. Surface modification of nanostructure lipid carrier (NLC) by oleoyl-quaternized-chitosan as a mucoadhesive nanocarrier. Colloids Surf. B Biointerfaces 149, 301–311.
Zhu, X.Y. et al., 2018. A Zebrafish heart failure model for assessing therapeutic agents. Zebrafish 15 (3), 243–253.
Zhang, N.H. et al., 2018a. Modulation of osteogenic and haemostatic activities by tuning cationicity of genipin-crosslinked chitosan hydrogels. Colloids Surf. B Biointerfaces 166, 29–36.
Zhang, Y., Chan, H.F., Leong, K.W., 2013. Advanced materials and processing for drug delivery: the past and the future. Adv. Drug Deliver. Rev. 65 (1), 104–120.
Zhang, Z.Y. et al., 2018b. Sandwich-like fibers/sponge composite combining chemotherapy and hemostasis for efficient postoperative prevention of tumor recurrence and metastasis. Adv. Mater. 30 (49), 1803217.